Mon. Not. R. Astron. Soc. **320**, 365–378 (2001)

Particle reacceleration in the Coma cluster: radio properties and hard X-ray emission

G. Brunetti,[1,2] G. Setti,[1,2] L. Feretti[2] and G. Giovannini[3,2]

[1]*Dipartimento di Astronomia, Università di Bologna, via Ranzani 1, I–40127 Bologna, Italy*
[2]*Istituto di Radioastronomia del CNR, via Gobetti 101, I–40129 Bologna, Italy*
[3]*Dipartimento di Fisica, Università di Bologna, via Berti–Pichat 6/2, I–40127 Bologna, Italy*

Accepted 2000 August 11. Received 2000 July 27; in original form 1999 December 10

ABSTRACT

The radio spectral index map of the Coma halo shows a progressive steepening of the spectral index with increasing radius. Such a steepening cannot be simply justified by models involving continuous injection of fresh particles in the Coma halo or by models involving diffusion of fresh electrons from the central regions.

We propose a two-phase model in which the relativistic electrons injected in the Coma cluster by some processes (starbursts, AGNs, shocks, turbulence) during a *first phase* in the past are systematically reaccelerated during a *second phase* for a relatively long time ($\sim$1 Gyr) up to the present time. We show that for reacceleration time-scales of $\sim$0.1 Gyr this hypothesis can well account for the radio properties of Coma C. For the same range of parameters which explain Coma C we have calculated the expected fluxes from the inverse Compton scattering of the Cosmic Microwave Background (CMB) photons, finding that the hard X-ray tail discovered by *BeppoSAX* may be accounted for by the stronger reacceleration allowed by the model.

The possibility of extending the main model assumptions and findings to the case of the other radio haloes is also discussed, the basic predictions being consistent with the observations.

Key words: acceleration of particles – radiation mechanisms: non-thermal – galaxies: clusters: general – galaxies: clusters: individual: Coma – radio continuum: general – X-rays: general.

1 INTRODUCTION

The intracluster medium (ICM) consists not only of the hot gas emitting thermal X-rays, but also of magnetic fields and relativistic particles. The existence of cluster magnetic fields and relativistic electrons is directly demonstrated by the presence of diffuse non-thermal radio emission detected in a number of clusters, the so-called radio haloes. Furthermore, Faraday rotation measurements toward discrete radio sources in clusters, coupled with the X-ray emission from the hot ICM, have indicated the presence of $\sim\mu$G magnetic field strengths.

The radiative lifetime of the relativistic electrons, mainly due to inverse Compton (IC) losses with the cosmic microwave background (CMB) photons, is relatively short ($\sim 10^{7-8}$ yr) so that the radio haloes suggest the presence of relatively fresh injected and/or reaccelerated electrons in the cluster volume (Jaffe 1977; De Young 1992; Tribble 1993; Brunetti et al. 1999). In general, models which assume a primary origin of the relativistic electrons require continuous injection processes and predict synchrotron radio emission and IC emission in the EUV and hard X-rays (Ensslin et al. 1997; Ensslin, Lieu & Biermann 1999; Sarazin 1999; Völk & Atoyan 1999), while secondary electron models skip the problem of the reacceleration (Dennison 1980; Blasi & Colafrancesco 1999) and predict large gamma-ray fluxes from neutral pion decay which could be tested by future gamma-ray missions.

Among halo sources, Coma C in the Coma cluster is the most famous and well-studied example of diffuse radio emission in cluster of galaxies, and it can be used to test the different models of radio halo formation and evolution.

At the lowest frequencies the radio emission of Coma C extends up to $\sim$30–40 arcmin from the centre (e.g. Cordey 1985 at 151 MHz; Hanisch & Erickson 1980 at 43 MHz; Henning 1989 at 30.9 MHz); at higher frequencies sensitive radio images have been obtained at 327 MHz (Venturi, Giovannini & Feretti 1990) and at 1.38 GHz (Kim et al. 1990). By applying Gaussian fits, it has been found that the 327-MHz FWHM (28×20 arcmin^2) is significantly larger than that at 1.38 GHz (18.7×13.7 arcmin^2), but smaller than the low-frequency size. The total radio spectrum of the Coma halo is steep ($\alpha \sim 1.2$), and the 327–1380 MHz spectral index

map shows that the spectrum steepens rapidly with increasing distance from the centre (Giovannini et al. 1993); the steepening has also been confirmed by 1.4-GHz data from the Effelsberg single-dish 100-m telescope (Deiss et al. 1997).

In principle, current models invoking a continuous injection of relativistic electrons may explain the total synchrotron spectrum of Coma C, but they fail to reproduce the spectral steepening with radius (Ensslin, Lieu & Biermann 1999; Völk & Atoyan 1999). Here it is important to realize that the diffusion velocity of the relativistic particles is low in relation to their radiative lifetimes, so that the spectral steepening cannot be related to the diffusion of rapidly ageing electrons from the central regions into the cluster volume (Berezinsky, Blasi & Ptuskin 1997; Sarazin 1999). As a consequence, unless one is ready to accept the rather unphysical scenario of an injection modulated across the cluster volume, the spectral steepening must be related to the intrinsic evolution of the local electron spectrum and to the radial profile of the cluster magnetic field strength.

Additional information of great importance in constraining the models of Coma C can also be obtained from observations at higher frequencies. Recently, Fusco-Femiano et al. (1999) have discovered an hard X-ray tail exceeding the thermal emission. Also in this case the existing models are not able to reconcile an IC origin of the hard X-ray flux with the estimates magnetic field intensities derived from rotation measure (RM) measurements, the required field being at least one order of magnitude weaker than the RM estimates (e.g. Ensslin, Lieu & Biermann 1999; Sarazin 1999, and references therein). This has stimulated alternative proposals for the origin of the hard X-ray excess (Dogiel 2000; Blasi 2000; Blasi, Olinto & Stebbins 2000; Ensslin 2000, and references therein).

In view of these difficulties, we investigate the alternative possibility and potentiality of a two-phase scenario for Coma C in which relativistic particles injected during a *first phase* are then reaccelerated during a *second phase*, possibly associated with a recent merger event as indicated by optical and X-ray observations. A preliminary, much simplified version of the model has been presented elsewhere (Brunetti et al. 1999). Here radiation and Coulomb losses and reacceleration efficiency are fully taken into account as a function of the cluster radius, and the assumption of a constant magnetic field throughout the cluster volume is released. A detailed description of the time evolution of the electron spectra is a distinctive feature of our model as compared to other current models (see, e.g., Sarazin 1999 and Ensslin 2000 for reviews).

The main aims of the present work are to:

(i) investigate the effects of energy losses and reacceleration gains on the energy distribution of the relativistic electrons, and find out whether the radio spectral steepening may significantly constrain the space of parameters of the physical processes at work in Coma C;

(ii) obtain the radial trend of the magnetic field strength for the same range of the physical parameters in (i) and compare it with the available information, and

(iii) compare the derived IC emission of Coma C with the hard X-ray flux measured by *BeppoSAX*, and find out whether the relatively high central values of the magnetic field indicated by the RM results are compatible with the IC scenario.

In Section 2 we introduce the model; Section 3 is devoted to a general presentation of the time evolution of the electron energy distribution subject to reacceleration and losses; the results concerning the radio properties of Coma C are given in Section 4, while those concerning the hard X-rays are given in Section 5. In Section 6 we discuss our findings and extend the model for Coma C to the case of the other haloes, and also summarize our main conclusions. In Appendix A we present a more detailed discussion of the theoretical aspects of the model. $H_0 = 50\,\mathrm{km\,s^{-1}\,Mpc^{-1}}$ is assumed throughout.

2 THE TWO-PHASE MODEL

2.1 The radio spectral steepening

By assuming a spherical symmetry of the relevant physical quantities and a Gaussian spatial profile of the emission coefficient, Deiss et al. (1997) have derived relationships between the observed and intrinsic spectral index distributions of the synchrotron emission. In the case of the Coma halo, they have shown that the FWHMs and flux densities of the radio observations (Kim et al. 1990; Venturi et al. 1990) can be reproduced by a central intrinsic spectral index $\alpha \sim 0.2$–0.4, leading to a central observed spectral index $\alpha \sim 0.7$, in agreement with Giovannini et al. (1993) findings. In Fig. 1 we plot the observed and intrinsic spectral indices predicted from Deiss et al. (1997) relationships based on the measurements at 327 MHz (Venturi et al. 1990), 1.38 GHz (Kim et al. 1990) and 1.4 GHz (Deiss et al. 1997). Both the data at 1.38 GHz (obtained with a synthesis radio telescope) and those at 1.4 GHz (obtained with a single-dish radio telescope), when combined with the 327-MHz data, show a marked steepening of the observed spectrum with distance from the centre; this confirms that the steepening in the Giovannini et al. (1993) spectral index map is not due to flux density losses at 1.38 GHz, but it is real. The points reported in Fig. 1 are taken from three slices across the halo centre of the spectral index map (Giovannini

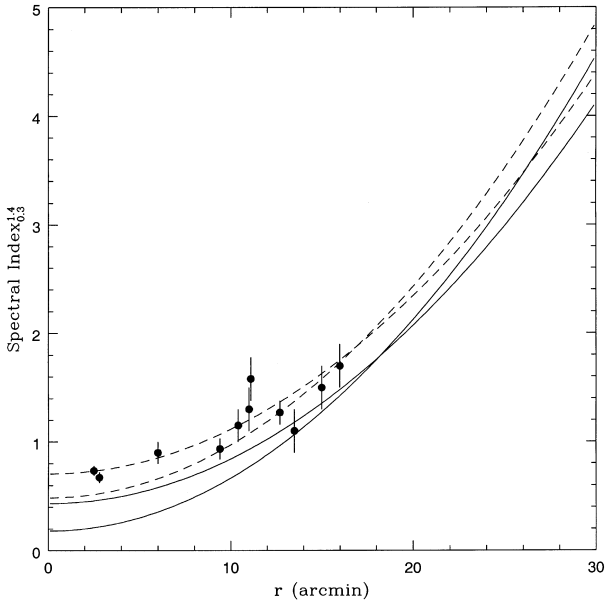

Figure 1. The predicted observable (dashed lines) and intrinsic (solid lines) spectral indices for the Coma halo are reported as a function of the distance from the centre. The curves are obtained from the Deiss et al. (1997) relationships based on 327/1380 MHz (bottom dashed and solid lines at $r = 0$) and 327/1400 MHz (single-dish) observations. The points are taken from three slices of the spectral index map (327–1380 MHz) of Giovannini et al. (1993) across the halo centre.

et al. 1993). Although there is some scattering, the agreement between the observed and derived spectral distributions is fairly good.

2.2 Injection phase

We investigate the application of a two-phase model for Coma C. During the *first phase* fresh particles are continuously injected in the volume of the Coma cluster for a sufficiently long time. An injection *phase* in the past can be reasonably related to starburst activity, during which violent galactic winds can accelerate relativistic particles (Zirakashvili et al. 1996; Ptuskin et al. 1997), and/or to the activity of AGNs producing a large amount of relativistic particles (Giovannini et al. 1993; Sarazin 1999). In addition, the high temperature of the ICM suggests that the ICM has passed through strong shocks, possibly during major mergers events when a significant portion of the shock energy can be channelled into the acceleration of relativistic particles (Blandford & Eichler 1987; Jones & Ellison 1991). Moreover, it is also possible that during major mergers relic particles, released in the past from starbursts and AGN activity, can be reaccelerated and injected at higher energies.

The time evolution of the particle energy distribution during the injection, $N(\gamma,t)$, is obtained by solving the kinetic equation (e.g. Kardashev 1962):

$$\frac{\partial N(\gamma,\theta,t)}{\partial t} = -\frac{\partial}{\partial \gamma}\left[\frac{\mathrm{d}\gamma}{\mathrm{d}t}N(\gamma,\theta,t)\right] + Q_{\mathrm{inj}}(\gamma,\theta,t), \quad (1)$$

with $Q_{\mathrm{inj}}(\gamma,\theta,t)$ being the injection function.

Following Sarazin (1999, fig. 1), we assume that the cooling of the relativistic electrons is dominated by Coulomb (ξ) and radiation [$\gamma^2\beta(z,\theta)$] losses, the relativistic bremsstrahlung being negligible, so that

$$\frac{\mathrm{d}\gamma}{\mathrm{d}t} = -\xi - \beta(\theta,z)\gamma^2. \quad (2)$$

The Coulomb losses depend on the ICM density as (e.g. Sarazin 1999)

$$\xi \simeq 1.2\times10^{-12}n\left[1+\frac{\ln(\gamma/n)}{75}\right] \sim 1.4\times10^{-12}n\,\mathrm{s}^{-1}, \quad (3)$$

while the coefficient of the radiative losses is

$$\beta(\theta,z) = 1.9\times10^{-9}[B^2\sin^2\theta + B_{\mathrm{IC}}^2(z)]\,\mathrm{s}^{-1}, \quad (4)$$

where θ is the pitch angle, z the redshift, and B_{IC} the equivalent magnetic field strength of the CMB.

If the particles are isotropically injected, i.e., $Q_{\mathrm{inj}}(\gamma,\theta) = Q_{\mathrm{inj}}(\gamma)/(4\pi)$, the only dependence of the electron spectrum on the pitch angle is given by the synchrotron loss term (equation 4). If the pitch-angle scattering is an efficient process, then the electrons are continuously isotropized; the term $B^2\sin^2\theta$ should be replaced by $2/3B^2$, and the solution is isotropic, i.e., $N(\gamma,\theta) = N(\gamma)/(4\pi)$.

The IC losses depend on the redshift as $(1+z)^4$, so that the cooling time of the relativistic electrons in clusters is expected to be dominated by the IC process at moderate and high redshifts; this produces a rapid ageing of fresh particles injected at $z > 0.3$ (Sarazin 1999). Due to the presence of reacceleration that dominates the time evolution of the electrons during the *second phase*, and since it starts less than $\sim$1 Gyr before the corresponding cluster age, in our model the dependence on z of the radiative losses is not important and has been neglected in the calculations.

Since the injection phase is assumed to hold in the past for a time considerably longer than the cooling time of the electrons, the energy distribution approaches a stationary spectrum (Sarazin 1999). Under stationary conditions and assuming a time-independent $Q_{\mathrm{inj}} = K_{\mathrm{e}}\gamma^{-\delta}$, equations (1) and (2) yield

$$N(\gamma,\theta) = \frac{K_{\mathrm{e}}}{\beta(\theta)(\delta-1)}\gamma^{-\delta+1}\left[\gamma^2+\frac{\xi}{\beta(\theta)}\right]^{-1}, \quad (5)$$

which is $\propto\gamma^{-\delta+1}$ at low energies (where Coulomb losses dominate) and $\propto\gamma^{-\delta-1}$ at higher energies where radiative losses dominate.[1]

2.3 Reacceleration phase

When the injection of fresh particles is stopped or strongly reduced, the energy distribution rapidly steepens and the number of high-energy radio-emitting electrons rapidly decreases.

In order to avoid the problem of the rapid ageing, we investigate the possibility that some reacceleration in the cluster volume is present during a *second phase* lasting less than about 1 Gyr up to the present cluster age. The presence of reacceleration mechanisms in cluster of galaxies has been pointed out by many authors studying the spectral ageing in head–tail radio sources (e.g. Jaffe & Perola 1973; Ekers et al. 1978; Fanti et al. 1981; Parma et al. 1999).

As a simplification of the scenario, we assume that the *second phase* starts when the efficiency of the injection processes is strongly reduced or stopped. The general case in which the end of the injection and the start of the reacceleration do not coincide is given in Appendix A; the main results remain unchanged. The *second phase* may be related to a merger or a post-merger scenario in which shocks and cluster weather, powered by the energy released during a merger, can compensate at some level for the radiative and Coulomb losses. A number of authors have found evidence for recent merging in the Coma cluster (Briel, Henry & Boheringer 1992; Vikhlinin, Forman & Jones 1997). Although we discuss specifically the case of Coma C, the radio haloes are generally found in clusters with recent merger activity (e.g. Feretti & Giovannini 1996); the general application of the two-phase model to the radio haloes is discussed in Section 6.2.

If the observed radio spectral steepening is related to the intrinsic evolution of the local electron energy distribution rather than to an unphysical injection modulation, important constraints on the physical processes at work in Coma C can be immediately obtained.

Indeed, the spectral steepening implies that the break of the synchrotron spectrum is in the range 0.3–1.4 GHz for a relevant fraction of the cluster volume. By making use of the basic synchrotron relationships, this immediately yields a typical break energy of the electron spectrum at $\gamma_{\mathrm{b}} \sim 10^4(B_{\mu\mathrm{G}})^{-1/2}$ and a radiative lifetime $T \sim 5\times10^{15}(B_{\mu\mathrm{G}})^{1/2}$ s for relatively weak magnetic fields (i.e., $B < B_{\mathrm{IC}} \sim 3\,\mu$G). Therefore, in order to generate Coma C, the reacceleration during the *second phase* must essentially balance the radiation losses, i.e., the reacceleration efficiency should be $\chi \sim 1/T \sim 2\times10^{-16}/\sqrt{B_{\mu\mathrm{G}}}\,\mathrm{s}^{-1}$. Moreover, a significant flattening of the relic electron distribution may only be attained for a reacceleration time τ such that electrons of energy $\gamma \sim 100$ are accelerated to $\sim\gamma_{\mathrm{b}}$ (see Section 3 for details and equation 6), so that $\tau > \ln(\gamma_{\mathrm{b}}/100)\chi^{-1} \sim 0.6$–$0.7$ Gyr.

[1] We will assume $\delta = 2.5$ throughout this paper.

If the average magnetic field intensity depends on the radial distance r from the cluster centre, it clearly follows that a reacceleration efficiency $\chi(r) \propto 1/\sqrt{B(r)}$ would produce a constant radio spectrum throughout the cluster. By allowing for a likely decrease of B with r, it then follows that a constant reacceleration efficiency results in a systematic steepening of the synchrotron spectrum with r, simply because at a given frequency higher energy electrons are selected by the lower field intensity. This steepening effect would be enhanced if the reacceleration efficiency increases in the regions of stronger fields. On the other hand, Coulomb losses are particularly severe in the central region of the cluster, leading to a marked flattening of the electron spectrum at low energies and, consequently, to a flattening of the synchrotron spectrum at low frequencies, as observed.

The above qualitative description of the effects of systematic reacceleration and losses on the evolution of the electron spectrum will be discussed in detail in Section 3. (Readers specifically interested in the application of the model to Coma C may skip this section and go directly to Section 4.)

3 EVOLUTION OF THE ELECTRON AND SYNCHROTRON SPECTRA

In this section we illustrate the time evolution of the electron energy distribution and related synchrotron spectra for a wide range of the relevant physical parameters. This provides the basic quantitative scenario delimiting the region of the parameter space which produces a self-consistent picture of the emission from Coma C.

3.1 The electron spectrum

As a simplification we assume that the particles are systematically reaccelerated by first-order Fermi mechanisms. The time evolution of the energy of the electrons is

$$\frac{\mathrm{d}\gamma}{\mathrm{d}t} = -\beta(\theta)\gamma^2 - \xi + \chi\gamma - \eta(\gamma)\gamma, \tag{6}$$

where χ expresses the efficiency of the reacceleration, and $\eta(\gamma)$ the relativistic bremsstrahlung losses given by (e.g. Sarazin 1999)

$$\eta(\gamma) \simeq 1.5\times10^{-16} n[\ln(\gamma) + 0.36]\,\mathrm{s}^{-1}. \tag{7}$$

Given the typical cluster thermal density $n \sim 10^{-3}\,\mathrm{cm}^{-3}$, the bremsstrahlung losses are always $\sim$100 times lower than the reacceleration efficiencies adopted in this work, and will be neglected.

With the initial ($t = t_\mathrm{i}$) spectrum given by equation (5), the solution of the kinetic equation (equation 1 with $Q = 0$) is

$$N(\gamma,\tau,\theta) = \frac{K_\mathrm{e} q(\theta)}{\delta-1}\frac{[1-\tanh^2(\tau\sqrt{q}/2)]\gamma^{-\delta+1}}{[2\gamma_\mathrm{b}(\tau,\theta)\tanh(\tau\sqrt{q}/2)]^2\beta^3(\theta)} \times\left[1-\frac{\gamma}{\gamma_\mathrm{b}(\tau,\theta)}\right]^{\delta-3}\left[1+\frac{\xi\gamma^{-1}-\chi}{\gamma_\mathrm{b}(\tau,\theta)\beta(\theta)}\right]^{-\delta+1} \times\left[\gamma^2\left\{\frac{1+(\xi\gamma^{-1}-\chi)[\gamma_\mathrm{b}(\tau,\theta)\beta(\theta)]^{-1}}{1-\gamma/\gamma_\mathrm{b}(\tau,\theta)}\right\}^2+\frac{\xi}{\beta(\theta)}\right]^{-1}, \tag{8}$$

where $q(\theta) = \chi^2 - 4\xi\beta(\theta)$ ($q > 0$; see Appendix A), $\tau = t - t_\mathrm{i}$, and γ_b is the break energy (i.e., the largest energy of the electrons) given by

$$\gamma_\mathrm{b}(\tau,\theta) = \frac{1}{2\beta(\theta)}\left(\chi + \frac{\sqrt{q}}{\tanh\dfrac{\tau\sqrt{q}}{2}}\right). \tag{9}$$

For $\xi = 0$ (no Coulomb losses) one finds $\gamma_\mathrm{b}(\theta) = \chi/\beta(1 - \mathrm{e}^{-\chi\tau})$ in agreement with Kardashev's (1962) results.

An example of the evolution with time of the energy distribution of the electrons is represented in Fig. 2 for $\chi = 2.0\times10^{-16}\,\mathrm{s}^{-1}$ (i.e., a reacceleration time $\simeq 1.6\times10^8$ yr) and $\xi = 1.3\times10^{-15}\,\mathrm{s}^{-1}$ (i.e., a thermal gas density $n \sim 10^{-3}\,\mathrm{cm}^{-3}$).

Due to the radiative losses, the high-energy part of the distribution evolves rapidly with time. When the break energy γ_b reaches the asymptotic value $(\chi + \sqrt{q})/2\beta$, the radiation losses are balanced by the reacceleration and the break energy is frozen; when τ becomes sufficiently larger than the reacceleration time, the combined effects of Coulomb losses and systematic reacceleration cause a depletion of the low-energy side of the electron energy distribution which rapidly flattens.

In Fig. 3 we report the electron energy distribution after a representative time interval $\tau = 0.8$ Gyr for different reacceleration efficiencies. As expected, one finds that stronger reaccelerations yield higher energy breaks and flatter energy distributions.

The effect on the particle energy distribution due to the increase of the Coulomb losses is illustrated in Fig. 4 for a given reacceleration. By increasing the ICM density, the Coulomb break in the initial spectrum is positioned at larger γs, causing a larger flattening of the electron spectrum at lower energies (equation 5), so that the reaccelerated spectrum is also flatter. At this point it should be noticed that, since the ICM density falls down with increasing distance from the centre, the electron energy distribution is also expected to be flatter in the central regions of the clusters.

The effect of increasing the radiative losses is illustrated in Fig. 5 for a given reacceleration. As expected, the balance

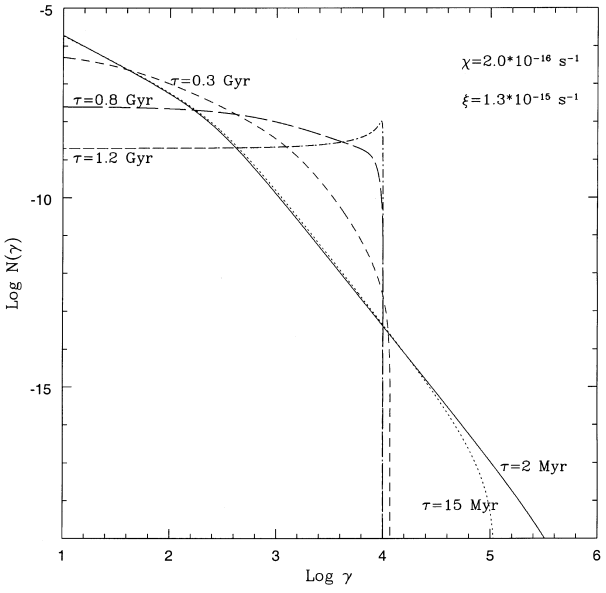

Figure 2. The predicted electron energy distribution is shown in arbitrary units as a function of the reacceleration period τ as indicated in the panel. The calculations are performed from equation (8) for $\chi = 2.0\times10^{-16}\,\mathrm{s}^{-1}$, $\xi = 1.3\times10^{-15}\,\mathrm{s}^{-1}$ and $B = 0.0$.

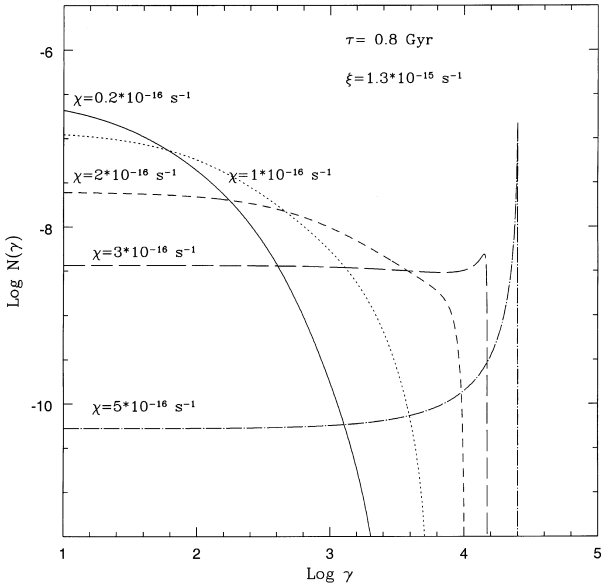

Figure 3. The predicted electron energy distribution is shown in arbitrary units as a function of the reacceleration efficiency as indicated in the panel. The calculations are performed from equation (8) for $\tau = 0.8\,\mathrm{Gyr}$, $\xi = 1.3 \times 10^{-15}\,\mathrm{s}^{-1}$ and $B = 0.0$.

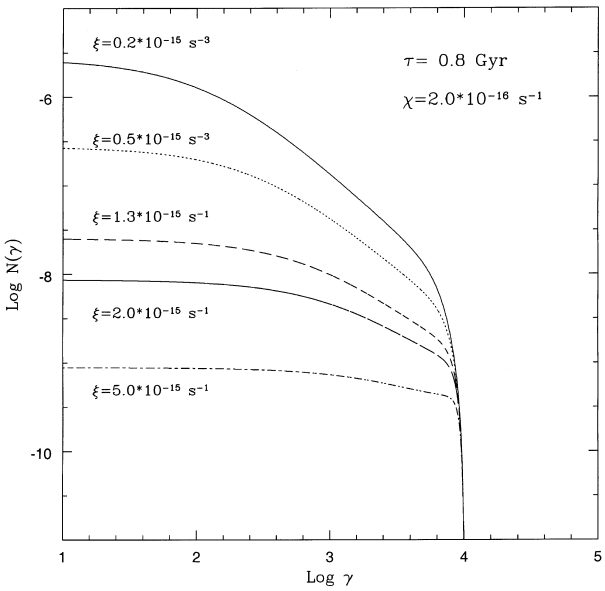

Figure 4. The predicted electron energy distribution is shown in arbitrary units as a function of the Coulomb losses as indicated in the panel. The calculations are performed from equation (8) for $\chi = 2.0 \times 10^{-16}\,\mathrm{s}^{-1}$, $\tau = 0.8\,\mathrm{Gyr}$ and $B = 0.0$.

between losses and reacceleration is obtained at lower energies with increasing B. Furthermore, with increasing B the break energy γ_b becomes closer to the energy at which the reacceleration balances the Coulomb losses and the energy distribution slightly flattens.

All these findings hold in general: in the case of systematic reacceleration of relativistic electrons in a thermal medium (as in clusters of galaxies) after a time sufficiently large, which depends on the reacceleration and/or losses, the electron energy distribution is expected to be flat or slightly inverted before a sharp cut-off.

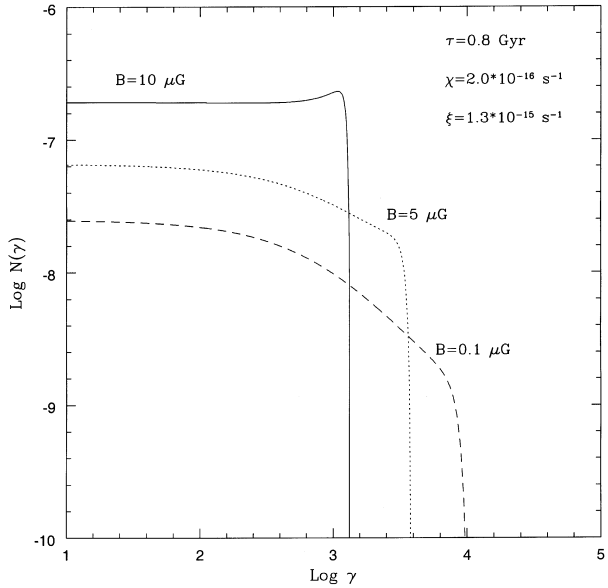

Figure 5. The predicted electron energy distribution is shown in arbitrary units as a function of the magnetic field strength B as indicated in the panel The calculations are performed from equation (8) for $\chi = 2.0 \times 10^{-16}\,\mathrm{s}^{-1}$, $\xi = 1.3 \times 10^{-15}\,\mathrm{s}^{-1}$, $\theta = 55°$ and $\tau = 0.8\,\mathrm{Gyr}$.

3.2 The synchrotron spectrum

In general, the synchrotron emissivity is obtained by integrating the synchrotron kernel over the electron energy and angular distributions (cf. Westfold 1959; Pacholczyk 1970). We assume that the electron momenta are isotropically distributed, and that the fields are tangled and of constant intensity on a sufficiently small scale. These assumptions allow us to consider the synchrotron emissivity (averaged over a sufficiently large volume) isotropic. By omitting, for simplicity of notation, the dependences of the functions, the emissivity per unit solid angle is

$$
\begin{aligned}
j\left(\frac{\nu}{\nu_\mathrm{b}}, \tau\right) = {} & \frac{K_\mathrm{e}}{\delta - 1}\frac{\sqrt{3}}{4}\frac{e^3}{mc^2}B\int_0^{\pi/2}\mathrm{d}\theta \sin^2\theta \phi(\theta) \\
& \times \int_0^1 \mathrm{d}u F\left(\frac{\nu/\nu_\mathrm{b}}{u^2\sin\theta}\right)(1-u)^{\delta-3}u^{-\delta+1} \\
& \times \left[1 + \frac{\xi u^{-1} - \chi\gamma_\mathrm{b}(\theta)}{\beta(\theta)\gamma_\mathrm{b}^2(\theta)}\right]^{-\delta+1} \\
& \times \left[u^2\left\{\frac{1 + [\xi u^{-1} - \chi\gamma_\mathrm{b}(\theta)]/[\gamma_\mathrm{b}^2(\theta)\beta(\theta)]}{1-u}\right\}^2 \right. \\
& \left. + \frac{\xi}{\beta(\theta)\gamma_\mathrm{b}^2(\theta)}\right]^{-1} \qquad (10)
\end{aligned}
$$

where the electron kernel

$$
F(y) = y\int_y^\infty K_{\frac{5}{3}}(v)\,\mathrm{d}v, \qquad (11)
$$

$K_{\frac{5}{3}}$ being the 5/3-order modified Bessel function,

$$
\phi(\theta) = q(\theta)\frac{1 - \tanh^2(\tau\sqrt{q}/2)}{[\tanh(\tau\sqrt{q}/2)]^2}\gamma_\mathrm{b}(\theta,\tau)^{-(\delta+2)}\beta^{-3}(\theta), \qquad (12)
$$

$$u(\theta) = \frac{\gamma}{\gamma_b(\theta,\tau)} = C\frac{B^2\sin^2\theta + B_{IC}^2}{\chi + \sqrt{q(\theta)}/\tanh\left(\frac{\tau\sqrt{q}}{2}\right)}\gamma, \quad (13)$$

$C \simeq 3\times10^{-9}$ cgs, and ν_b the critical frequency calculated for $\gamma = \gamma_b$ ($\theta = 90°$).

As it is well known, the shape of the synchrotron spectrum depends on the electron distribution in the 3D momentum space; this is a function of the combined losses and reaccelerations (equation 8). The IC losses are constant over the cluster volume, but both the magnetic field B and the Coulomb losses are expected to vary with the distance r from the centre. Thus the relativistic electron energy distribution (equation 8), the break energy and the importance of the synchrotron losses with respect to the IC losses depend on r. As a consequence, the shape of the synchrotron spectrum (equations 10 and 12) depends on r, and it is expected to be intermediate between those calculated in the case of pure synchrotron losses (Kardashev 1962; Pacholczyk 1970; Komissarov & Gubanov 1994: the KP-model) and of pure IC losses (Jaffe & Perola 1973; Komissarov & Gubanov 1994: the JP-model).

As discussed in the preceeding section, increasing the Coulomb losses and/or the systematic reacceleration yields, in general, a flattening in the energy distribution of the relativistic electrons. The effects on the synchrotron spectrum are illustrated in Fig. 6 for given τ and B. As expected, the synchrotron spectrum below the break frequency becomes flatter with increasing the ICM density and/or the systematic reacceleration. It should also be noticed that the synchrotron spectra are not sensitive to the presence of spectral spikes in the electron energy distribution (Fig. 3). If stochastic Fermi mechanisms provide a substantial contribution to the reacceleration of the electrons, the spectral spikes are expected to be smoothed out, but our results remain unchanged.

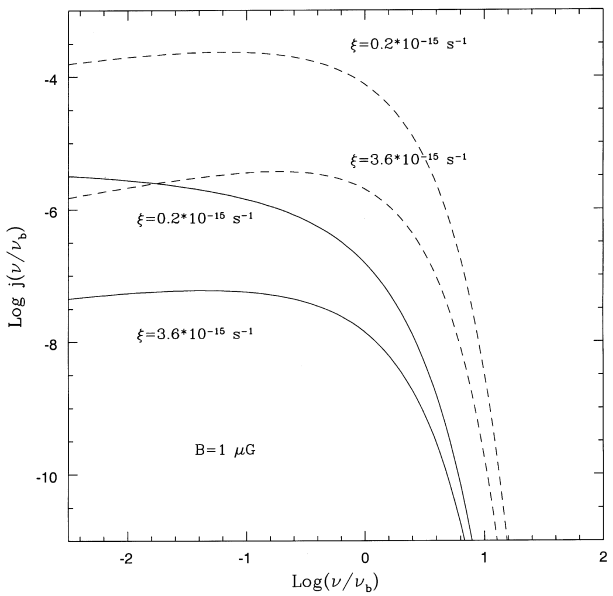

Figure 6. The predicted synchrotron spectrum is shown in arbitrary units for two well-separated values of the Coulomb losses as indicated in the panel. The frequency scale is in unit of the break frequency ν_b. We assume two reacceleration efficiencies: $\chi = 2.5\times10^{-16}\,s^{-1}$ (solid lines) and $\chi = 4.2\times10^{-16}\,s^{-1}$ (dashed lines). The calculations are performed for a reacceleration period $\tau = 0.8$ Gyr and $B = 1.0\,\mu$G (typical for the Coma centre).

4 MODEL RESULTS FOR COMA C

As shown in the previous section, a natural consequence of the combined reacceleration and Compton losses is the flattening of the electron spectrum and of the related synchrotron emission in the central region of a cluster, in qualitative agreement with what is actually found in Coma C. In this section the physical parameters will be constrained in order to reproduce the observed spectral steepening and total radio spectrum.

4.1 Basic assumptions

Following Deiss et al. (1997), we approximate the brightness distribution at each frequency with a symmetric Gaussian of FWHM $\Delta(\nu)$ equal to the geometric mean of the smaller and larger FWHM measured at each frequency. The very rapid decrease of the radio brightness given by the Gaussian approximation cannot well constrain the synchrotron electron distribution at large distances from the cluster centre where the brightness fades into the noise. Thus, in the model computation, the tail of this distribution should be allowed to vary within the observational uncertainties. To this end, we model the radio brightness distribution by adding to the Gaussian from the fits at each observed frequency a symmetric Gaussian of larger FWHM $\Delta_l(\nu)$ so that the observed emissivity is represented by

$$j^{obs}(r,\nu) = A(\nu)\times\left\{e^{-\left[\frac{r}{0.6\Delta(\nu)}\right]^2} + f e^{-\left[\frac{r}{0.6\Delta_l(\nu)}\right]^2}\right\}, \quad (14)$$

$A(\nu)$ giving the normalization of the radio brightness distribution, and f being a free parameter (from the radio maps we find $f \leq 0.06$).

As shown in the preceding section, the Coulomb losses play an important role in shaping the electron energy distribution and the associated synchrotron spectrum. By adopting the β-model of Briel et al. (1992), the Coulomb losses are

$$\xi(r) = 4.2\times10^{-15}\left[1+\left(\frac{r}{R_C}\right)^2\right]^{-3\beta/2}, \quad (15)$$

where $R_C = 10.5$ arcmin is the core radius of the ICM, and $\beta = 0.75$ (the central density is $n_0 \simeq 3\times10^{-3}\,cm^{-3}$).

We assume that the efficiency of the reacceleration can be parametrized as the sum of a constant large-scale component and a small-scale component. Indeed, turbulent gas motion originating from the massive galaxies orbiting in the cluster can amplify the efficiency of the large-scale reacceleration within the cluster core (Deiss & Just 1996). As a possible choice, we assume that the small-scale reacceleration is roughly proportional to the inverse of the typical distance between galaxies. By adopting the observed galaxy distribution in the Coma cluster (Girardi et al. 1995), we parametrize the reacceleration as

$$\chi(r) = \chi_{LS} + \chi_{G0}\left[1+\left(\frac{r}{R_G}\right)^2\right]^{-\alpha_G/3}, \quad (16)$$

$R_G = 5.5$ arcmin being the optical core radius, and $\alpha_G = 0.8$.

It should be noticed, however, that since the radio brightness and the spectral properties of the model are obtained by integrating the emissivities over the cluster volume, the main model results do not depend strongly on the precise choice of the functional dependence in equation (16).

In the sequel we adopt a reacceleration time interval $\tau = 0.8$ Gyr, but we anticipate that the essential features of the model are not modified as long as τ is of the order of 1 Gyr.

Finally, we assume complete reisotropization of the electron momenta, not only for simplicity, but also because the pitch-angle scattering is likely to be an efficient process during the reacceleration *phase*. We have carried out several tests and found that, due to the low magnetic field intensities, the differences between the synchrotron spectrum (and all the other relevant quantities in this paper) calculated in the isotropic and anisotropic cases are negligible.

4.2 Matching the observations: the inferred *B* field distribution

From equations (10)–(16), at each r and for a given set of the parameters ($\chi_{\rm LS}$, $\chi_{\rm G0}$ and B), we obtain the synchrotron emissivity as a function of the frequency measured in terms of the break frequency $\nu_{\rm b}(r)$ [$\nu_{\rm b}(r) \propto B(r)\gamma_{\rm b}^2(r;\theta = 90°)$], and then we can compute the spectral index between 327 MHz and 1.4 GHz.

In Fig. 7 we plot the calculated intrinsic spectral index between 327 MHz and 1.4 GHz at $r = 5$ arcmin as a function of B and for different values of the reacceleration efficiency χ. Small values of B lead to very steep radio spectra, because the break frequency of the synchrotron spectrum is comparable to, or smaller than, 327 MHz. Moderate values of the magnetic field allow us to obtain very flat spectra like those derived for the central regions of the Coma halo ($\alpha_{0.3}^{1.4} \sim 0.4$–$0.5$ at $r = 5$ arcmin). Since from simple synchrotron relationships the break frequency is $\nu_{\rm b} \propto B(B_{\rm IC}^2 + B^2)^{-2}$, it is found that the value of B for which the spectral index is the smallest for any given reacceleration χ is obtained when $B \sim B_{\rm IC} \simeq 3\,\mu$G, while the value of B for which one obtains a given spectral index depends on χ.

The magnetic field $B(r)$ is numerically derived by imposing that the calculated spectral index matches the intrinsic one of Fig. 1 (the average between Deiss et al. 1997 and Giovannini et al. 1993 curves). The results are shown in Fig. 8 for relevant values of the reacceleration parameters. For relatively small distances from the cluster centre the value of the magnetic field is sensitive to the assumption about both $\chi_{\rm LS}$ and $\chi_{\rm G}$, while at larger distances, due to the rapid decrease of the small-scale reacceleration efficiency (equation 15), the value of B depends only on $\chi_{\rm LS}$.

With reference to Fig. 7 and $\alpha = 0.5$, we find a lower bound to the central value of the reacceleration efficiency $\chi(0) \sim 3.3 \times 10^{-16}\,{\rm s}^{-1}$ and a corresponding magnetic field strength $B(0) \sim 3\,\mu$G which is the largest value of the central field intensity compatible with our model.

We emphasize that these results depend only on the radio spectral indices and not on the normalizations of the relativistic electron distributions.

The magnetic field strength required by our model to match the spectral indices in the central region can be compared with the values given in the literature, obtained by Faraday rotation measurements. Kim et al. (1990) have estimated a magnetic field $B = (1.7 \pm 0.9)\,\mu$G in the central regions of the Coma cluster, assuming a tangling scale of the magnetic field of 10–40 kpc. More recently, Feretti et al. (1995), studying the RM distribution of the head–tail radio source NGC 4869 located near the centre of Coma, inferred the existence of a strong magnetic field component ($B \sim 6\,\mu$G) tangled on the kpc scale. The two values are not in conflict, considering that the 6-μG field could be associated to the local environment around NGC 4869. The value obtained by our model in the central Coma region ($\sim$ 1–3 μG) is consistent with the above measurements. It is also in agreement with the results of Clarke, Kronberg & Böringer (1999), who, using statistical RM technique in a sample of low-redshift, rich Abell clusters, find central values of the magnetic field of the order of a few μG.

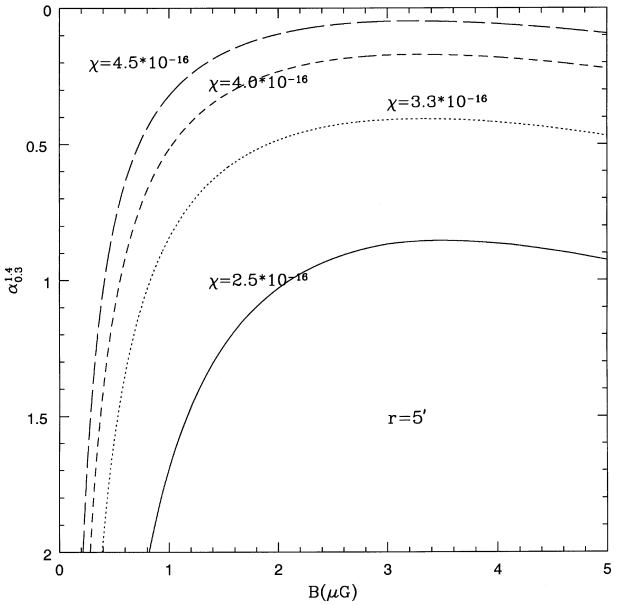

Figure 7. The calculated 0.327–1.4 GHz spectral index is given as a function of the magnetic field B at a distance $r = 5$ arcmin. The calculations are performed for several reacceleration parameters χ as indicated in the panel, and for the value of ξ obtained from equation (15). The reacceleration time interval is $\tau = 0.8$ Gyr.

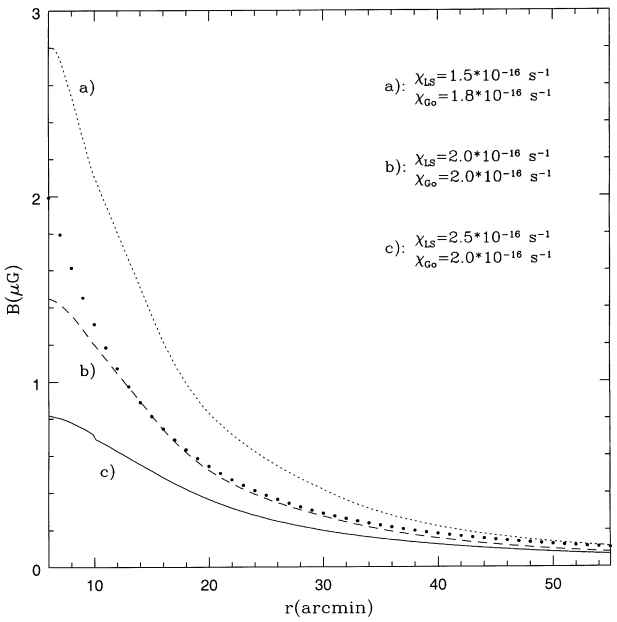

Figure 8. The B distribution required by the model to match the spectral observations is reported for different reaccelerations as indicated in the panel. The calculations are performed for a reacceleration period $\tau = 0.8$ Gyr. Due to the reacceleration profile (equation 16) the magnetic field in the majority of the cluster volume depends only on $\chi_{\rm LS}$. The dots represents the Jaffe (1980) theoretical predictions for the magnetic field distribution in the Coma cluster (we have assumed $B_0 = 3\,\mu$G).

The RM results can be used to constrain the reacceleration parameter from above. With reference to Fig. 7, we find that the central value of the magnetic field is significantly smaller than 1 μG for $\chi(0) > 5 \times 10^{-16}\,\mathrm{s}^{-1}$, setting an upper bound to the reacceleration efficiency in our model.

The origin and structure of the magnetic fields in galaxy clusters are presently debated. Seed fields could be generated by turbulent galactic wakes (Jaffe 1980) and/or by ejecta from galaxies (Kronberg, Lesch & Lepp 1999; Völk & Atoyan 1999), and maintained by turbulent dynamo driven by galaxy motions through the ICM (De Young 1992). Such low-level magnetic fields can also be amplified by cluster mergers (Norman & Bryan 1998; Eilek 1999). According to Jaffe (1980), the magnetic field distribution depends on the thermal gas density (n) and on the distribution of massive galaxies (n_G) as $B(r) = B(0)[n(r)/n(0)]^{0.5}[n_G(r)/n_G(0)]^{0.4}$. Jaffe (1980) predictions calculated for the Coma cluster, adopting $B(0) \sim 3\,\mu$G and with $n(r)$ from Briel et al. (1992) and $n_G(r)$ from Girardi et al. (1995), are consistent with our model findings (Fig. 8).

4.3 The predicted total synchrotron spectrum

The model at this point is anchored to the observed and intrinsic 327–1400 MHz spectral index distribution as a function of r, and to the observed FWHMs of the brightness distribution at these frequencies.

The spectral shape of the synchrotron emission at a given radius is very different from a simple relatively steep power law such as the total Coma C radio spectrum. The shape of the electron energy distribution changes with r in a predictable way depending on losses and gains which, as shown in Section 4.2, are now well constrained.

As a consequence, a fundamental test of the model is whether it can reproduce the observed total synchrotron spectrum. This is obtained by integrating the synchrotron emissivity (equation 10) over the cluster volume, taking into account the r-dependence of the parameters involved in the calculation. It is at this point that the electron spectra are normalized as a function of r in order to match the *observed* emissivities (equation 14) derived from the brightness distributions at 327 and 1400 MHz, following the Deiss et al. (1997) procedure. As an illustrative example, in Fig. 10 we plot the electron energy distribution at different distances from the cluster centre for the representative case c) of Fig. 8.

The calculated total synchrotron spectra for the same set of parameters as in Fig. 8 are represented in Fig. 9 and compared with the observations. Once the uncertainties in the observations are considered, the model well accounts for the observed radio spectrum over all the frequency range sampled by the observations. Since the model is mainly forced on the 327- and 1400-MHz observations, it is not surprising that the computed spectra between these two frequencies are essentially indistinct. On the contrary, at higher and lower frequencies the calculated synchrotron spectrum is more sensitive to the assumed parameters. In order to see whether this effect can help in further constraining the model parameters, it is important to assess the quality of the spectral measurements.

The radio fluxes quoted in the literature are obtained by subtracting from the observed fluxes those contributed by point sources falling within the halo. Since the observations at different frequencies have been performed with very different instruments and, in some cases, at times differing of many years, the subtraction of the sources is not standard and can influence the calculation of the halo flux. In particular, the low-frequency points at 43 and 74 MHz in Fig. 9 were obtained by subtracting the extrapolated flux from 5C4.81 and 5C4.85, and a contributed flux from the unresolved sources measured at 430 MHz and extrapolated down to low frequencies (Hanisch & Erickson 1980); the 30.9-MHz halo flux has been obtained by subtracting all the sources from the 151-MHz survey with an extrapolated flux density at 30.9 MHz larger than 1 Jy (Henning 1989). More

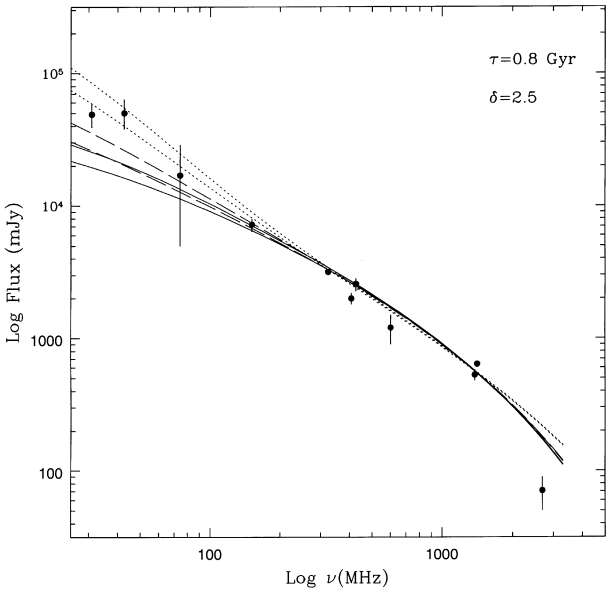

Figure 9. The total synchrotron radio spectrum predicted by our model is compared with the flux measurements for the three model with parameters specified in Fig. 8: model a) (dotted lines), model b)(dashed lines) and model c)(solid lines). The calculations are given for two different values of f (equation 16): 0.01 (lower lines), 0.02 (upper lines).

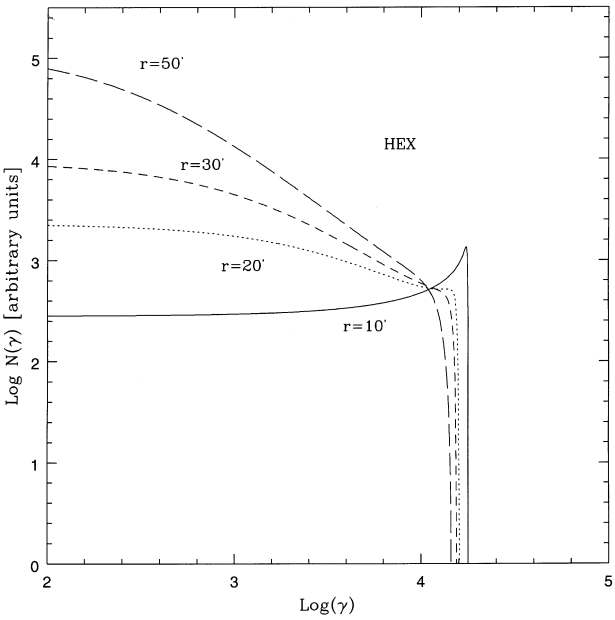

Figure 10. The electron energy spectra are reported at different distances from the cluster centre (normalization scale in arbitrary units). The calculations are performed for model c) with $f = 0.015$ (Fig. 8). The energy interval of the electrons emitting hard X-rays via IC scattering of the CMB photons is also shown (HEX).

precise subtraction procedures have been applied at higher frequencies thanks to the better spatial resolution: the 327-MHz radio flux of the Coma halo has been obtained by subtracting the 327-MHz flux densities from a list of 64 unresolved sources observed at 327 and/or 1400 MHz (Venturi et al. 1990), and a similar procedure has been adopted by Deiss et al. (1997) at 1.4 GHz by using the list of radio sources as compiled by Kim et al. (1994) (the 2.7-GHz flux is likely to be underestimated; Deiss et al. 1997). We find that the detailed high-frequency subtractions are deeper than those performed at lower frequencies by 20–40 per cent, so that the 30.9-, 43- and 74-MHz fluxes reported in Fig. 9 may be considered as upper limits. It follows that the low-frequency data cannot discriminate among the models in Fig. 9.

In our model the radio spectrum at low frequencies ($\nu <$ 100 MHz) is dominated by the contribution of the radiation emitted at large radii ($r >$ 12–17 arcmin). The contribution from the particle with very low break frequencies at $r >$ 30–35 arcmin, not detected in the high-frequency maps due to ageing, is also important. Larger values of f, corresponding to an increased number of particles at large distances from the centre, do not appreciably modify the 327–1400 MHz spectrum, but increase the low-frequency radio fluxes expected by the model (Fig. 9).

By increasing the large-scale reacceleration ($\chi_{\rm LS}$), the spectrum of the synchrotron electrons is depressed and the expected radio fluxes at low frequencies decrease (Fig. 9). On the other hand, by decreasing $\chi_{\rm LS}$ the low-frequency radio spectrum steepens and may significantly overproduce the observations (Fig. 9). This allows us to obtain a range for the large-scale reacceleration efficiency of $1.5 \times 10^{-16} < \chi_{\rm LS} < 3 \times 10^{-16}\,{\rm s}^{-1}$. Accurate measurements at low frequencies, such as those obtainable with the VLA at 74 MHz, are of crucial importance to constrain the model parameters.

Due to the very steep radio spectrum of the external regions, the high-frequency spectrum of the Coma halo does not depend on f (Fig. 9). It is emitted by regions at $r <$ 12 arcmin and depends on both the large-scale and small-scale reacceleration efficiencies. With increasing reacceleration in the cluster core the particle spectrum flattens and the break energy increases: this causes a decrease of the required B value, so that the 327-MHz emitted frequency is closer to the synchrotron break frequency. As a net consequence the high-frequency radio spectrum steepens (Fig. 9).

4.4 Relic electrons and halo energetics

The shape of the injection rate (projected) of the relic electron population, $K_{\rm e}(r)$, is shown in Fig. 11. It has been obtained by inverting the synchrotron emission equations for model (c) in Fig. 8 (the integral of equation 10 along the line of sight). The shape is rather close, within a factor ~2, to both the thermal and galaxy number density distributions in Coma. This result is very encouraging, since no quantitative assumptions on the space distribution of the relic electrons have been made in the derivation of the model. However, the similarity with the matter distribution is consistent with our conjecture that relativistic particles must have been efficiently injected into the ICM during the *first phase* by AGN and galaxy activity.

The total energy associated with the relativistic electrons in the cluster is the result of the energy injected during the *first phase*, and of the energy gained by the electrons during the *second phase*. We find that for a reacceleration parameter $\chi \sim 3 \times 10^{-16}\,{\rm s}^{-1}$ the total energy in relativistic electrons is $\sim 10^{59}$ erg.

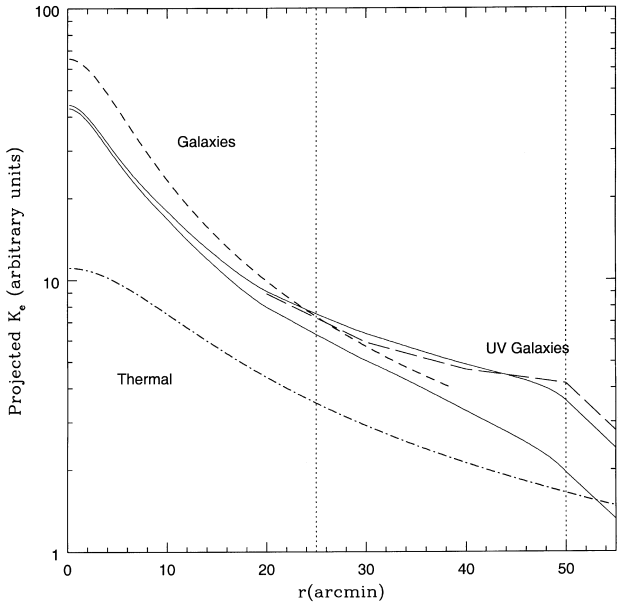

Figure 11. The projected distribution of the injection rate of the relativistic electrons $K_{\rm e}(r)$ (equation 5) during the *first phase* is given (solid lines) as a function of r (in arcmin) for model (c) in Fig. 8 ($f = 0.01$ and 0.02, starting from the bottom). The shapes of the projected density of the thermal gas (obtained from Briel et al. (1992) fit) and of the galaxies (Girardi et al. 1995) (dashed lines) are conveniently scaled for a closer comparison; the projected galaxy density profile is valid only up to 38 arcmin from the cluster centre. The projected radial distribution of the UV galaxies (Donas et al. 1995), normalized to the Girardi et al. counts, is also plotted for $r >$ 20 arcmin. The region in which the 80–90 per cent of the IC hard X-ray flux is produced during the *second phase* (Section 5) is enclosed by the vertical dotted lines.

We point out that this value is much smaller (by a factor >10) than that associated with the relativistic electron population considered in the other proposed models (Kempner & Sarazin 1999, and references therein). This is because the rather flat electron energy spectrum, characteristic of our model, is much more efficient than those of the other models in emitting synchrotron radiation at radio wavelengths.

5 THE HARD X-RAY TAIL IN THE COMA CLUSTER

From a deep *BeppoSAX* observation Fusco-Femiano et al. (1999) discovered a hard X-ray tail, in the range 20–80 keV, exceeding the extrapolation of the thermal X-ray emission spectrum; this excess has also been confirmed by an *RXTE* observation (Rephaeli, Gruber & Blanco 1999) with consistent results. Due to the poor statistics, the spectrum is not well constrained, so that the origin of this high-energy emission cannot be firmly established. Several models have been explored. It can be generated by the IC scattering of the radio-emitting electrons with the CMB photons (Sarazin & Lieu 1998; Fusco-Femiano et al. 1999; Sarazin 1999); in this case, models invoking a secondary production of the electrons yield a gamma-ray flux considerably larger than the *EGRET* upper limit (Blasi & Colafrancesco 1999). Alternatively, it might originate via relativistic bremsstrahlung of a suprathermal power-law tail of particles (Ensslin et al. 1999), or, as proposed by Dogiel (2000) and Blasi (2000), emitting from the thermal emission of a modified

Maxwellian distribution of the hot ICM induced by strong acceleration processes ($\chi \sim 1.5 \times 10^{-15}\,\mathrm{s}^{-1}$, Dogiel 2000).

The IC origin is particularly attractive, in view of the fact that a comparison between the radio emission from the halo and the hard X-ray tail discovered by *BeppoSAX*, if spatially coincident, may allow a direct estimate of the average strength of the magnetic field B over the cluster volume. Nevertheless, since in the present model the electron energy spectrum depends on the distance from the cluster centre (Fig. 10), the synchrotron as well as the IC spectra are emitted by relativistic electrons whose energy distribution cannot be represented by a unique power law over the whole volume. Therefore the magnetic field cannot be simply evaluated by standard formulae (e.g. Harris & Grindlay 1979).

Under our assumptions (equation 8) the IC emissivity per unit energy and solid angle in the ultrarelativistic Thompson approximation is given by

$$j(\epsilon_1, r) = \frac{2r_0^2\pi^2}{c^2h^3}\int\int_0^{\pi}\frac{\mathrm{d}\epsilon\mathrm{d}\theta\sin\theta}{\mathrm{e}^{\epsilon/kT_{\mathrm{CMB}}}-1}\int_{\gamma_{\min}}^{\gamma_{\mathrm{b}}(r,\tau,\theta)}\frac{\mathrm{d}\gamma}{\gamma^{\delta+3}} \times\left[1-\frac{\gamma}{\gamma_{\mathrm{b}}(r,\tau,\theta)}\right]^{\delta-3}\left[1+\frac{\xi(r)\gamma^{-1}-\chi(r)}{\gamma_{\mathrm{b}}(r,\tau,\theta)\beta}\right]^{-\delta+1} \times\left[\gamma^2\left\{\frac{1+[\xi(r)\gamma^{-1}-\chi(r)][\gamma_{\mathrm{b}}(r,\tau,\theta)\beta)]^{-1}}{1-\gamma/\gamma_{\mathrm{b}}(r,\tau,\theta)}\right\}^2 +\frac{\xi(r)}{\beta}\right]^{-1}\frac{K_{\mathrm{e}}(r)}{\delta-1}\mathcal{C}(r,\theta)K_{\mathrm{IC}}\left(\frac{\epsilon_1}{\epsilon},\gamma\right), \quad (17)$$

where

$$\mathcal{C}(r,\theta) = q(r,\theta)\frac{[1-\tanh^2(\tau\sqrt{q}/2)]}{[2\gamma_{\mathrm{b}}(r,\theta,\tau)\tanh(\tau\sqrt{q}/2)]^2}\beta^{-3}(r,\theta) \quad (18)$$

$$K_{\mathrm{IC}}\left(\frac{\epsilon_1}{\epsilon},\gamma\right) = \epsilon_1\left(2\epsilon_1\ln\frac{\epsilon_1}{4\gamma^2\epsilon}+\epsilon_1+4\gamma^2\epsilon-\frac{\epsilon_1^2}{2\gamma^2\epsilon}\right), \quad (19)$$

ϵ being the energy of the CMB photons and for ultrarelativistic electrons $\gamma_{\min} = \sqrt{\epsilon_1/4\epsilon}$ (e.g. Blumenthal & Gould 1970). As a cluster volume we assume a sphere of radius 55 arcmin (~2.2 Mpc), which is about the radius up to which the counts of UV galaxies, presumed cluster members, begin merging the background galaxies (Donas, Milliard & Laget 1995).

Since the IC emission is only sensitive to the number of electrons, it is expected to be mainly contributed by the outer parts $r > 30$ of the cluster volume which contain the large majority of the relativistic electrons able to IC scatter the CMB photons in the *BeppoSAX* hard band (Fig. 10). As a consequence, the predicted X-ray luminosity is sensitive to the large-scale reacceleration efficiency; we find that from 80 to 90 per cent of the model 20–80 keV flux is emitted between 30–50 arcmin from the centre (Fig. 11).

The calculated hard X-ray IC fluxes from our model for the three choices of the parameters given in Fig. 8 are compared with the *BeppoSAX* data in Fig. 12. Models with relatively high reacceleration efficiencies may account for a large fraction or all of the X-ray flux measured by *BeppoSAX*. By comparing Fig. 12 with Fig. 9, it is seen that it is precisely this type of models that contribute less to the synchrotron flux at very low radio frequencies. It is not surprising, then, that in order not the overproduce the *BeppoSAX* flux, we obtain an upper limit for the large-scale reacceleration efficiency $\chi_{\mathrm{LS}} < 3 \times 10^{-16}\,\mathrm{s}^{-1}$, the same as that found in Section 4.3. Obviously, accurate measurements at low radio frequencies would be of crucial importance not only to constrain the parameters of our model for Coma C, but also to check whether an IC origin of *BeppoSAX* hard X-rays is viable. Thus, at variance with statements found in the literature, central magnetic fields of ~1 μG may be consistent with an IC origin of the *BeppoSAX* hard X-ray flux, the reason being that while the X-rays are mainly produced in the outer regions of the cluster, the radio flux above a few 100 MHz is mainly produced in the inner regions.

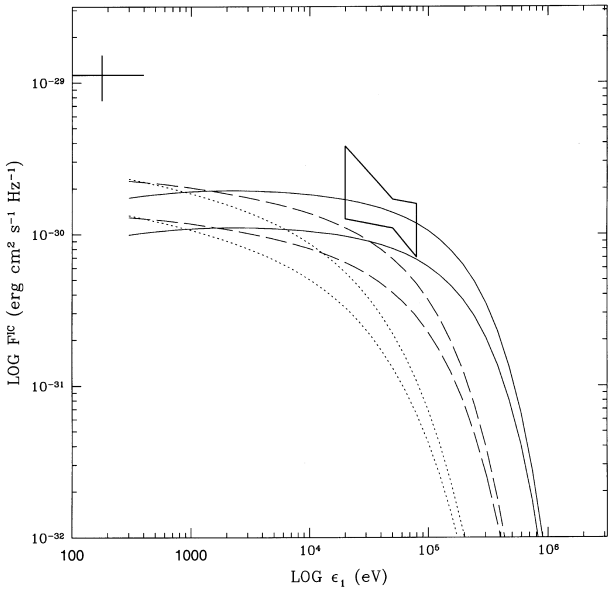

Figure 12. The IC fluxes from the Coma cluster for the three models in Fig. 8 (lower line $f = 0.01$, upper line $f = 0.02$). The *BeppoSAX* hard X-ray data are obtained from Fusco-Femiano et al. (1999), with the spectral indices at the 90 per cent confidence level; a 15 per cent uncertainty in the normalization is assumed. The cross represents the Coma EUV excess Bowyer et al. (1999).

In Fig. 12 we have also represented the EUV flux from Bowyer, Berghöfer & Korpela (1999): the model EUV flux is well below the observed. The origin of the EUV excess is still unclear, its spatial distribution is considerably narrower than the radio brightness distribution and, if non-thermal, it is probably associated to an additional electron population (Bowyer & Berghöfer 1998; Brunetti et al. 1999; Ensslin et al. 1999).

6 DISCUSSION AND CONCLUSIONS

6.1 A two-phase model for Coma C

It has been shown that the radio properties of Coma C can be explained by a two-phase model consisting of an injection period, in which a power-law spectrum of relativistic electrons has been continuously injected throughout the cluster volume and modified by radiative and Coulomb losses, followed by a reacceleration phase of the aged (relic) spectrum for typical duration of ~1 Gyr up to the present time.

The model is anchored to the spectral index map of Coma C between 327 and 1400 MHz, which shows a marked steepening going in the outward direction from a flat central value. The explanation of this pattern, not accounted for in other published models, constitutes the basic motivation of this work.

On the basis of simple considerations (Section 2.3) we have shown that the reacceleration efficiency should be

$\chi \sim 2 \times 10^{-16}\,\mathrm{s}^{-1}$, and the reacceleration time $\tau > 0.6\,\mathrm{Gyr}$. A detailed modelling has then been worked out based on the following assumptions.

(i) The brightness distributions at 327 and 1400 MHz are described as the sum of two Gaussians; the radio images constrain the peak amplitude of the large-scale Gaussian to be a fraction $f < 0.06$ of that of the small-scale Gaussian. By assuming a spherical symmetry, the emissivities at 327 and 1400 MHz and the corresponding spectral index as a function of the radial distance r are obtained from the observed brightness distributions by making use of Deiss et al.'s (1997) procedure.

(ii) The Coulomb losses, $\xi(r)$, are fixed by the β-model fit of the ICM of Briel et al. (1992).

(iii) The reacceleration efficiency is assumed to be represented by the sum of two terms: a large-scale reacceleration (χ_{LS}) constant throughout the cluster volume and a small-scale reacceleration [$\chi_{\mathrm{G}}(r)$] peaking at the cluster centre. We have identified the large-scale component with shocks and/or turbulence, possibly generated during a recent merger, and the small-scale component with the amplification of such shocks/turbulence by the motion of the massive galaxies in the cluster core.

(iv) The relic electron population is allowed to evolve, subject to radiation and Coulomb losses, for a reacceleration time $\tau = 0.8\,\mathrm{Gyr}$.

With these assumptions we find the following.

(1) The electron energy distribution depends on r, being much flatter and with a somewhat higher energy break toward the cluster centre, where both the magnetic field intensity and the reacceleration parameter are stronger and the Coulomb losses are more severe.

(2) The value of the 327–1400 MHz spectral index in the central region ($\alpha = 0.5$) implies an upper bound to the intensity of the magnetic field $B \sim 3\,\mu\mathrm{G}$ and a lower bound to the reacceleration efficiency $\chi(0) \sim 3.3 \times 10^{-16}\,\mathrm{s}^{-1}$.

(3) A central magnetic field of at least $1\,\mu\mathrm{G}$, as indicated by RM measurements, implies an upper bound to the reacceleration efficiency at the centre of $\chi(0) \sim 5 \times 10^{-16}\,\mathrm{s}^{-1}$.

(4) By fitting the steepening of the 327–1400 MHz spectral index with r, the magnetic field intensity smoothly tapers off from central values of 1–3 μG to ~0.05–0.1 μG at $r \sim 50$ arcmin.

(5) The model synchrotron emission perfectly fits the total radio spectrum of Coma C within 327 and 1400 MHz, independent of the χ and f parameters allowed to vary within the limits set above. This demonstrates the internal consistency of the model. On the contrary, the computed low-frequency fluxes vary appreciably with the parameters, being higher with decreasing χ and increasing f: most of this flux is emitted by the outer parts of the cluster volume, so that by a closer comparison with the observed low-frequency flux it is possible to set limits on the large-scale acceleration efficiency $1.5 \times 10^{-16} < \chi_{\mathrm{LS}} < 3 \times 10^{-16}\,\mathrm{s}^{-1}$.

(6) With the electron energy and space distributions constrained by the radio data it is found that the X-rays produced by IC scattering the CMB photons can account for the hard X-ray flux discovered by *BeppoSAX* if the larger figures of the χ_{LS} and f parameters, allowed by the radio model, apply. Like the flux emitted at low radio frequencies, most of the X-rays are produced in the outer volume of the cluster. This demonstrates once again the crucial importance of accurate flux measurements at frequencies <100 MHz. We remark that the *BeppoSAX* flux is significantly overproduced for $\chi_{\mathrm{LS}} > 3 \times 10^{-16}\,\mathrm{s}^{-1}$ ($f = 0.02$), which is consistent with the upper limit set by the radio spectrum at low frequencies.

(7) By de-evolving the electron spectra constrained by the radio model, it is found that the shape of projected radial distribution of the injection rate of the relic electron population is very similar to that of the galaxies in the Coma cluster. This is consistent with our conjecture that the relic electron population may have been injected by AGN and galaxy activity at earlier epochs.

(8) The present energy in relativistic electrons required by our model is $\sim 10^{59}$ erg, at least 10 times smaller than in other proposed models. The energy budget required at the end of the injection phase is $\sim 2 \times 10^{58}$ erg, if almost immediately followed by the reacceleration phase, and becomes larger by increasing the time gap between the two-phases, simply because the spectrum of the relic electrons is further depressed. We find that a temporal gap of 3–4 Gyr involves an energy budget ~100 times larger, but still reasonable (see Appendix A).

We emphasize that the results listed above are obtained essentially by imposing that the model accounts for the radio properties of Coma C, and we find that this requirement is already stringent enough to constrain the relevant parameters, such as the reacceleration's efficiencies and time, within a narrow range. We also notice that the typical reacceleration efficiency, corresponding to an e-folding time-scale of ~0.1 Gyr, is relatively modest and comparable to, or smaller than, the values frequently quoted both in clusters (cluster weathering) and in tailed radio galaxies.

Finally, the likely presence of relativistic protons injected with the electrons deserves some attention. It can be constrained by looking for the gamma-ray emission from the decay of the π^0 generated in the p–p collisions. Recently, Blasi & Colafrancesco (1999) have worked out a secondary electron model for Coma C, and estimated an upper bound $\sim 4 \times 10^{63}$ erg ($H_0 = 50\,\mathrm{km\,s^{-1}\,Mpc^{-1}}$) for the total energy of centrally injected protons in order not to exceed the upper limit on the gamma-ray flux set by *EGRET* (this figure should be much larger in our model, where the majority of the relativistic particles are injected in regions of low ICM density). Since in our model the particle reacceleration is due to shocks and/or turbulence in the ICM, the energy gained by relativistic protons during the *second phase* cannot exceed the thermal energy of the ICM ($\sim 10^{63}$ erg), so that the gamma-ray flux from p–p collisions in our model is expected to be far below the *EGRET* limit.

6.2 General considerations for the radio haloes

Although the present work is focused on Coma C, we believe that a *two-phase* model may explain the radio properties of other haloes as well.

As for Coma, the required energy input in the ICM could be supplied by a recent merger, as suggested by the evidence of a significant association between radio haloes and cluster mergers. Moreover, it has been found that the occurrence of radio haloes in clusters increases with the cluster X-ray luminosity L_{X} in the 0.1–2.4 keV band (from ~4 per cent for $L_{\mathrm{X}} < 5 \times 10^{44}\,\mathrm{erg\,s^{-1}}$ to ~36 per cent for $L_{\mathrm{X}} > 10^{45}\,\mathrm{erg\,s^{-1}}$; Giovannini, Tordi & Feretti 1999). This is consistent with the expectations of the two-phase model, since more X-ray luminous, massive clusters would have produced a larger number of injected particles during the *first phase*, thus supplying sufficient energy for the formation of the radio haloes also after a moderately long gap between the injection and the reacceleration phases.

It should be borne in mind, however, that the strength of the halo radio emission will depend critically on the combination of the various parameters (reacceleration efficiency and duration, magnetic field strength and the temporal gap between the two-phases), so that we expect that only a fraction of the massive clusters with a recent merger will show a substantial radio halo. For instance, contrary to expectation a too efficient reacceleration may result in an electron spectrum very much stretched toward higher energies so that, other conditions being equal, there may be fewer relativistic electrons emitting at radio frequencies in a given magnetic field, and the halo emission would be dimmed.

The IC emission of the relativistic electrons with the CMB photons will typically fall in the UV and EUV band at the end of the injection phase, progressively moving toward the X-ray band during the reacceleration phase. Thus, non-thermal X-ray emission from clusters with recent mergers should be a quite common feature, depending on the total number of relic electrons. In general, as seen in the case of Coma, the radio at intermediate frequencies and the hard X-rays are expected to be mainly contributed by different regions: the former near the centre of the cluster, associated with regions of relatively higher B, and the latter from the outer parts of the cluster volume. Clearly, observations with future hard X-ray facilities will be of great value in checking the correctness of this scenario.

ACKNOWLEDGMENTS

We are grateful to A. Atoyan, S. Colafrancesco and T. Ensslin for useful discussions and to M. Murgia for providing a numerical table of the synchrotron electron kernel. We thank the referee whose criticism has stimulated us to work out an improved version of the paper. This work was partly supported by the Italian Ministry for University and Research (MURST) under grant Cofin98-02-32, and by the Italian Space Agency (ASI).

REFERENCES

Berezinsky V. S., Blasi P., Ptuskin V. S., 1997, ApJ, 487, 529
Blandford R., Eichler D., 1987, Phys. Rep., 154, 1
Blasi P., 2000, ApJ, 9, 532L
Blasi P., Colafrancesco S., 1999, APh, 12, 169
Blasi P., Olinto A. V., Stebbins A., 2000, ApJ, 535, L71
Blumenthal G. R., Gould R. J., 1970, Rev. Mod. Phys., 42, 237
Bowyer S., Berghöfer T. W., 1998, ApJ, 506, 502
Bowyer S., Berghöfer T. W., Korpela E., 1999, ApJ, 526, 592
Briel U. G., Henry J. P., Boheringer H., 1992, A&A, 259, L1
Brunetti G., Feretti L., Giovannini G., Setti G., 1999, in Böhringer H., Feretti L., Schuecker P., eds, Diffuse Thermal and Relativistic Plasma in Galaxy Clusters, MPE–Report 271
Clarke T. E., Kronberg P. P., Böringer H., 1999, in Böhringer H., Feretti L., Schuecker P., eds, Diffuse Thermal and Relativistic Plasma in Galaxy Clusters, MPE–Report 271
Cordey R. A., 1985, MNRAS, 215, 437
Deiss B. M., Just A., 1996, A&A, 305, 407
Deiss B. M., Reich W., Lesch H., Wielebinski R., 1997, A&A, 321, 55
Dennison B., 1980, ApJ, 239, L93
De Young D., 1992, ApJ, 386, 464
Dogiel V. A., 2000, A&A, 357, 66
Donas J., Milliard B., Laget M., 1995, A&A, 303, 661
Eilek J. A., 1998, in Böhringer H., Feretti L., Schuecker P., eds, Diffuse Thermal and Relativistic Plasma in Galaxy Clusters, MPE–Report, 271
Ekers R. D., Fanti R., Lari C., Ulrich M.-H., 1978, A&A, 69, 253
Ensslin T. A., 2000, Proc. IAU Symp. The Universe at Low Radio Frequencies, in press (astro-ph/0001433)
Ensslin T. A., Biermann P. L., Kronberg P. P., Wu X.-P., 1997, ApJ, 477, 560
Ensslin T. A., Lieu R., Biermann P. L., 1999, A&A, 344, 409
Fanti R., Lari C., Parma P., Ekers R. D., 1981, A&A, 94, 61
Feretti L., Giovannini G., 1996, in Ekers R., Fanti C., Padrielli L., eds, Proc. IAU Symp. 175, Extragalactic Radio Sources. Kluwer, Dordrecht, p. 333
Feretti L., Dallacasa D., Giovannini G., Tagliani A., 1995, A&A, 302, 680
Fusco-Femiano R. et al., 1999, ApJ, 513, L197
Giovannini G., Feretti L., Venturi T., Kim K. T., Kronberg P. P., 1993, ApJ, 406, 399
Giovannini G., Tordi M., Feretti L., 1999, New Astronomy, 4, 141
Girardi M., Biviano A., Giurcin G., Mardirossian F., Mezzetti M., 1995, ApJ, 438, 527
Kempner J. C., Sarazin C. L., 1999, ApJ, 512, 345
Kronberg P. P., Lesch H., Lepp U., 1999, ApJ, 511, 56
Hanisch R. J., Erickson W. C., 1980, AJ, 85, 183
Harris D. E., Grindlay J. E., 1979, MNRAS, 188, 25
Henning P., 1989, AJ, 97, 1561
Jaffe W. J., 1977, ApJ, 212, 1
Jaffe W. J., 1980, ApJ, 241, 925
Jaffe W. J., Perola G. C., 1973, A&A, 26, 423
Jones F. C., Ellison D. C., 1991, Space Sci. Rev., 58, 259
Kardashev N. S., 1962, SvA, 6, 317
Kim K. T., Kronberg P. P., Dewdney P. E., Landecker T. L., 1990, ApJ, 355, 29
Kim K. T., Kronberg P. P., Dewdney P. E., Landecker T. L., 1994, A&AS, 105, 385
Komissarov S. S., Gubanov A. G., 1994, A&A, 285, 27
Norman M. L., Bryan G. L., 1998, in Meisenheimer K., Röser H.-J., eds, Ringberg Workshop on M87, Springer Lecture Notes in Physics
Pacholczyk A. G., 1970, in Burbidge G., Burbidge M., eds, Radio Astrophysics. Freeman and Company, San Francisco
Parma P., Murgia M., Morganti R., Capetti A., De Ruiter H. R., Fanti R., 1999, A&A, 344, 7
Ptuskin V. S., Völk H. J., Zirakashvili V. N., Breitschwerdt D., 1997, A&A, 321, 434
Rephaeli Y., Gruber D., Blanco P., 1999, ApJ, 511, L21
Sarazin C. L., 1999, ApJ, 520, 529
Sarazin C. L., Lieu R., 1998, ApJ, 494, L177
Tribble P. C., 1993, MNRAS, 261, 57
Venturi T., Giovannini G., Feretti L., 1990, AJ, 99, 1381
Vikhlinin A., Forman W., Jones C., 1997, ApJ, 474, L7
Völk H. J., Atoyan A. M., 1999, APh, 11, 73
Westfold K. C., 1959, ApJ, 130, 241
Zirakashvili V. N., Breitschwerdt D., Ptuskin V. S., Völk H. J., 1996, A&A, 311, 113

APPENDIX A: THE GENERAL TWO-PHASE MODEL

In Section 3 we analysed the effect due to the systematic reacceleration on the energy distribution. In order to simplify the scenario, it was assumed that the reacceleration phase starts when the injection phase is stopped or strongly reduced.

In this appendix we generalize the results of this paper by assuming that the two-phases are separated in time.

After the injection is stopped at a given time t_i, we let the particles age for a time interval Δt. Mostly due to IC losses with the CMB photons, the particles age rapidly, and the energy distribution is depopulated at relatively high energies.

By integrating equation (2) with constant losses, one obtains

$$\gamma(\theta, \Delta t) = \frac{\gamma(t_i) - \sqrt{\xi/\beta(\theta)}\tan[\sqrt{\xi\beta(\theta)}\Delta t]}{1 + \gamma(t_i)\sqrt{\beta(\theta)/\xi}\tan[\sqrt{\xi\beta(\theta)}\Delta t]} \quad \text{(A1)}$$

and a break energy

$$\gamma_{\rm b,1}(\theta)=\frac{1}{\sqrt{\beta/\xi}\tan(\sqrt{\xi\beta}\Delta t)}. \quad \text{(A2)}$$

Then, from the kinetic equation (equation 1, with $Q=0$), one finds the energy distribution of the electrons:

$$N(\gamma,\Delta t,\theta)=\frac{K_{\rm e}[1+\tan^2(\sqrt{\beta\xi}\Delta t)]}{\beta(\theta)(\delta-1)}\left(1-\frac{\gamma}{\gamma_{\rm b,1}}\right)^{\delta-1}\times\left[\gamma+\frac{\xi}{\beta(\theta)\gamma_{\rm b,1}}\right]^{-(\delta+1)}\times\left\{1+\left[\frac{1-\gamma/\gamma_{\rm b,1}}{\gamma+\frac{\xi}{\beta(\theta)\gamma_{\rm b,1}}}\right]^2\frac{\xi}{\beta(\theta)}\right\}^{-1} \quad \text{(A3)}$$

which becomes equation (5) for $\Delta t\rightarrow 0$.

We assume that after a time Δt following the end of the injection phase, the particles are reaccelerated. The time evolution of the energy of the electrons is obtained by integrating equation (6):

$$\tau=\begin{cases} q<0\Rightarrow \\ \dfrac{2}{\sqrt{-q}}\left[\tan^{-1}\dfrac{\chi-2\xi\gamma(\tau)}{\sqrt{-q}}-\tan^{-1}\dfrac{\chi-2\xi\gamma(\Delta t)}{\sqrt{-q}}\right] \\ q>0\Rightarrow \\ \dfrac{-2}{\sqrt{q}}\left[\tanh^{-1}\dfrac{\chi-2\xi\gamma(\tau)}{\sqrt{q}}-\tanh^{-1}\dfrac{\chi-2\xi\gamma(\Delta t)}{\sqrt{q}}\right], \end{cases} \quad \text{(A4)}$$

where $q(\theta)=\chi^2-4\xi\beta(\theta)$ expresses the importance of the reacceleration.

Equation (A4) can be explicated in terms of γ; it gives

$$\gamma(\tau,\theta)=\frac{\sqrt{-q}}{2\xi}\frac{2\xi\gamma(\Delta t)-\chi-\sqrt{-q}\tan(x)}{[2\xi\gamma(\Delta t)-\chi]\tan(x)-\sqrt{-q}}+\frac{\chi}{2\xi} \quad \text{(A5)}$$

for $q<0$, while

$$\gamma(\tau,\theta)=\frac{\gamma(\Delta t)[\sqrt{q}/\tanh(x)+\chi]-2\xi}{2\beta(\theta)\gamma(\Delta t)+\sqrt{q}/\tanh(x)-\chi} \quad \text{(A6)}$$

for $q>0$,

$$x=\frac{\sqrt{|q|}}{2}\tau \quad \text{(A7)}$$

and τ is the reacceleration period. Equation (A6) reduces to equation (A1) for $\tau=0$. The break energies are obtained from equations (A5) and (A6) by imposing $\gamma(\Delta t)\rightarrow\infty$:

$$\gamma_{\rm b}(\tau,\theta)=\begin{cases} q<0\Rightarrow \\ \sqrt{-q}\,[2\xi\tan(x)]^{-1}+\chi/2\xi \\ q>0\Rightarrow \\ [\chi+\sqrt{q}/\tanh(x)][2\beta(\theta)]^{-1}. \end{cases} \quad \text{(A8)}$$

In the case of the Coma cluster, $q>0$; this is because by assuming a physically sound reacceleration time $\sim 10^8$ yr, it is $\chi^2\sim 10^{-31}$, while, given the thermal gas density and the IC losses, it is $4\xi\beta<4\times10^{-34}$. The energy distribution of the reaccelerated electrons is obtained by solving the kinetic equation (equation 1, with $Q=0$) with equations (A3), (A6) and (A8):

$$N(\gamma,\tau,\theta)=\frac{q(\theta)K_{\rm e}}{4}\frac{1-\tanh^{-2}(x)}{\beta^3(\theta)\gamma_{\rm b}^2(\theta)}\frac{1+\tan^2[\sqrt{\beta(\theta)\xi}\Delta t]}{\delta-1}\times\left[1-\frac{\gamma\mathcal{L}(\theta)}{\gamma_{\rm b,1}}\right]^{\delta-1}\times\left\{1+\left[\frac{1-\gamma\mathcal{L}(\theta)/\gamma_{\rm b,1}}{\gamma\mathcal{L}(\theta)+\frac{\xi}{\beta(\theta)\gamma_{\rm b,1}}}\right]^2\frac{\xi}{\beta(\theta)}\right\}^{-1}\times\left[\gamma\mathcal{L}(\theta)+\frac{\xi}{\beta(\theta)\gamma_{\rm b,1}}\right]^{-(\delta+1)}[1-\gamma/\gamma_{\rm b}(\theta)]^{-2}, \quad \text{(A9)}$$

where

$$\mathcal{L}(\theta)=\left[1+\frac{\xi\gamma^{-1}-\chi}{\gamma_{\rm b}(\theta)\beta(\theta)}\right]\left[1-\frac{\gamma}{\gamma_{\rm b}(\theta)}\right]^{-1}. \quad \text{(A10)}$$

The final shape of the energy distribution of the emitting electrons is mostly dependent on the reacceleration phase during which it is heavily modified. For this reason, even if the particles can be injected and age over cosmological time-scales, in the calculation of equation (A3) we have not considered the variation with z of the IC losses.

However, the final energy distribution, equation (A9), depends on Δt and on $\gamma_{\rm b,1}$ which are directly related to the redshift at the end of the injection phase and to the redshift at which the reacceleration phase starts; such dependences can be simply introduced in the model.

In the case of an Einstein–de Sitter universe, one has

$$\Delta t=\frac{2}{3H_0}[(1+z_{\rm acc})^{-3/2}-(1+z_{\rm i})^{-3/2}]. \quad \text{(A11)}$$

$z_{\rm i}$ is the redshift corresponding to the end of the injection phase, while $z_{\rm acc}$, the redshift corresponding to the start of the reacceleration phase, is given by

$$z_{\rm acc}=\left(1-\frac{3H_0\tau}{2}\right)^{-2/3}-1. \quad \text{(A12)}$$

If the particles age over cosmological time-scales, the IC losses are expected to dominate the Coulomb losses for $\gamma\geq 100$, so that equation (2) can be simplified and solved by considering the dependence of β on z and that $\mathrm{d}z/\mathrm{d}t=H_0\sqrt{1+z}$; one finds:

$$\gamma(z_{\rm acc})=\frac{\gamma(z_{\rm i})}{1+\frac{\beta}{H_0}b(z_{\rm i},z_{\rm acc}),} \quad \text{(A13)}$$

where

$$b(z_{\rm i},z_{\rm acc})=\tfrac{2}{3}[(1+z_{\rm i})^{5/2}-(1+z_{\rm acc})^{5/2}]; \quad \text{(A14)}$$

the break energy is simply obtained from equations (A13) and (A14) with $\gamma(z_{\rm i})\rightarrow\infty$:

$$\gamma_{\rm b,1}=\frac{3H_0}{2\beta}[(1+z_{\rm i})^{5/2}-(1+z_{\rm acc})^{5/2}]^{-1}. \quad \text{(A15)}$$

Given τ and $z_{\rm i}$, from equations (A12), (A15) and (A11) one has

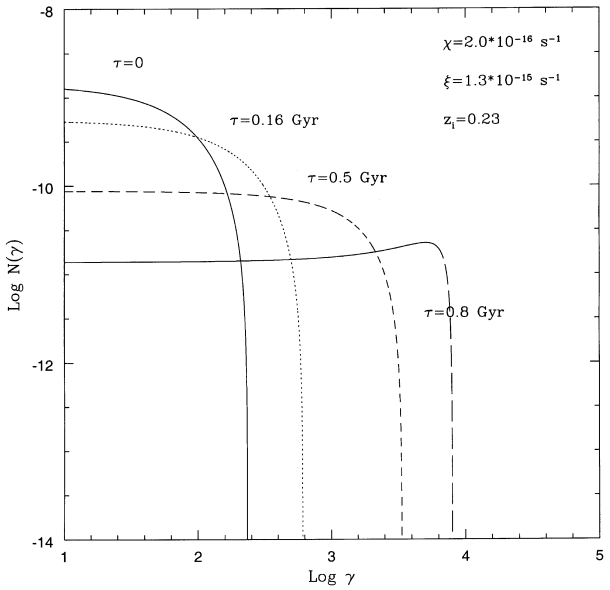

Figure A1. The predicted electron energy distribution, in the same arbitrary units as in Fig. 3, is shown as a function of the reacceleration period τ as indicated in the panel. The calculations are performed from equation (A9) for $\chi = 2.0 \times 10^{-16}\,\mathrm{s}^{-1}$, $\xi = 1.3 \times 10^{-15}$ and $z_\mathrm{i} = 0.23$. The parameters Δ and $\gamma_{\mathrm{b},1}$ can be calculated respectively from equations (A11) and (A15); one has 3.4 Gyr, 230 (solid line), 3.24 Gyr, 238 (dotted line), 2.9 Gyr, 255 (short-dashed line) and 2.6 Gyr, 271 (long-dashed line).

$\gamma_{\mathrm{b},1}$ and Δt; then from equation (A9) one has the particle energy distribution at $z = 0$.

In Fig. A1 the model energy distribution of relativistic electrons injected up to a redshift $z = 0.23$ is shown for different reacceleration times. The break of the electron energy distribution rapidly increases for a reacceleration time $\tau \leq 0.8$ Gyr, and then it reaches the asymptotic value of $\sim 10^4$. During the reacceleration the IC emission from such a population is expected to be channelled at the beginning in the UV, then in the soft X-rays, and finally in the hard X-rays.

By assuming that the energy released during a merger generates an efficient reacceleration of the order of $\sim 10^8$ yr in the cluster volume for ~ 1 Gyr, then non-thermal hard X-ray emission should be produced for ~ 0.5 Gyr.

The possibility of a gap between the two model phases gives a strong limit in the detection of non-thermal emission (either synchrotron and IC) from merging clusters. Depending on the gap duration, a considerable fraction of the electrons is thermalized or shifted at low energies (where the Coulomb losses dominate also during the reacceleration phase) after the *injection phase*.

We find that, if the gap is $\sim$ 3–4 Gyr long, the energy content of the relativistic electrons is reduced by a factor of ~ 100 (Figs 3 and A1).

This paper has been typeset from a TEX/LATEX file prepared by the author.